Solventless Synthesis of Bi_2S_3 (Bismuthinite) Nanorods, Nanowires, and Nanofabric

Michael B. Sigman, Jr. and Brian A. Korgel*

Department of Chemical Engineering, Texas Materials Institute, Center for Nano- and Molecular Science and Technology, The University of Texas at Austin, Austin, Texas 78712-1062

Received December 7, 2004. Revised Manuscript Received January 22, 2005

Orthorhombic Bi_2S_3 (bismuthinite) nanorods and nanowires are synthesized by the solventless thermolysis of bismuth alkylthiolate precursors. Reactions carried out in air at ∼225 °C in the presence of a capping ligand species, octanoate, produce high aspect ratio (>100) nanowires. Lower aspect ratio nanowires (∼7) are produced by the same approach with the addition of elemental sulfur at lower reaction temperature (∼160 °C). Both the nanowires and nanorods are oriented with their long axes in the [002] crystallographic direction. Higher reaction temperatures (∼250 °C) produce crossed nanowire networks, or fabrics, with highly oriented growth as a result of heterogeneous nanowire nucleation and epitaxial elongation off the surface of existing wires.

Introduction

General synthetic approaches for sterically stabilized nanocrystals with tunable composition, size, and shape are being developed to produce high-quality nanomaterials for fundamental studies and practical applications. Solution-phase, ligand-assisted arrested precipitation has been effective for many types of solids, including those with metallic, covalent, and ionic chemical bonding.[1] Size (and shape) distribution control remains the primary challenge in these syntheses as frequent interparticle collisions can lead to aggregative growth resulting in broad log-normal size distributions and significant concentrations of crystallographic defects in the particle cores.[2−5] Recently, we have explored nanocrystal arrested precipitation in the *absence of solvent*, thus eliminating interparticle diffusion and collisions during the growth process, which in principle should promote diffusion-limited particle growth and narrow size and shape distributions. Using this solventless approach, size- and shape-monodisperse metal sulfide nanocrystals—Cu_2S and NiS nanorods, nanodisks, and nanoprisms—have indeed been produced by thermally decomposing metal alkylthiolate precursors in the presence of octanoate.[6−8]

In this article, we demonstrate the solventless synthesis of crystalline *high aspect ratio* Bi_2S_3 nanowires from a bismuth (Bi) alkylthiolate precursor, and further show that the nanowire aspect ratio can be decreased significantly by increasing the relative availability of sulfur in the reaction. Bi_2S_3 is a photoconductive, direct band gap (E_g = 1.3 eV) semiconductor,[9,10] with numerous potential applications including photovoltaics,[9,11,12] sensors,[13] and thermoelectrics.[14,15] Several techniques have previously been reported for synthesizing elongated Bi_2S_3 nanocrystals including solvothermal[16−19] and hydrothermal[20−22] decomposition, microwave irradiation,[23] crystallization of amorphous colloids,[24] chemical vapor deposition,[18,25] and sonochemical methods,[26] but the solventless technique offers the advantage of forming highly crystalline rods or wires with well-defined surfaces and small average diameters (10.7 nm for nanorods and 26.0 nm for nanowires).

* Corresponding author. E-mail: korgel@che.utexas.edu. Tel: (512) 471-5633. Fax: (512) 471-7060.

(1) For a recent review, see *Semiconductor and Metal Nanocrystals: Synthesis and Electronic Properties*; Klimov, V. I., Ed.; Marcel Dekker: New York, 2004.
(2) Peng, Z. A.; Peng, X. *J. Am. Chem. Soc.* **2002**, *124*, 3343.
(3) Peng, X. *Adv. Mater.* **2003**, *15*, 459.
(4) LaMer, V. K.; Dinegar, R. H. *J. Am. Chem. Soc.* **1950**, *72*, 4847.
(5) Sugimoto, T. *Chem. Eng. Technol.* **2003**, *26*, 313.
(6) Larsen, T. H.; Sigman, M.; Ghezelbash, A.; Doty, R. C.; Korgel, B. A. *J. Am. Chem. Soc.* **2003**, *125*, 5638.
(7) Sigman, M. B.; Ghezelbash, A.; Hanrath, T.; Saunders: A. E.; Lee, F.; Korgel, B. A. *J. Am. Chem. Soc.* **2003**, *125*, 16050.
(8) Ghezelbash, A.; Sigman, M. B.; Korgel, B. A. *Nano Lett.* **2004**, *4*, 537.
(9) Grigas, J.; Talik, E.; Lazauskas, V. *Phys. Status Solidi B* **2002**, *232*, 220.
(10) Black, J.; Conwell, E. M.; Seigle, L.; Spencer, C. W. *J. Phys. Chem. Solids 2* **1957**, *2*, 240.
(11) Suarez, R.; Nair, P. K.; Kamat, P. V. *Langmuir* **1998**, *14*, 3236.
(12) Mane, R. S.; Sankapal, B. R.; Lokhande, C. D. *Mater. Chem. Phys.* **1999**, *60*, 158.
(13) Grigas, J.; Talik, E.; Lazauskas, V. *Phys. Status Solidi B* **2002**, *232*, 220.
(14) Chen, B.; Uher, C. *Chem. Mater.* **1997**, *9*, 1655.
(15) Cantarero, A.; Martinez-Pastor, J.; Segura, A. *Phys. Rev. B* **1987**, *35*, 9586.
(16) Wang, D.; Shao, M.; Yu, D.; Li, G.; Qian, Y. *J. Cryst. Growth* **2002**, *243*, 331.
(17) Liu, Z.; Peng, S.; Xie, Q.; Hu, Z.; Yang, Y.; Zhang, S.; Qian, Y. *Adv. Mater.* **2003**, *15*, 936.
(18) Koh, Y. W.; Lai, C. S.; Du, A. Y.; Tiekink, E. R. T.; Loh, K. P. *Chem. Mater.* **2003**, *15*, 4544.
(19) Yu, S.; Qian, Y.; Shu, L.; Xie, Y.; Yang, L.; Wang, C. *Mater. Lett.* **1998**, *35*, 116.
(20) Zhang, W.; Yang, Z.; Huang, X.; Zhang, S.; Yu, W.; Qian, Y.; Jia, Y.; Zhou, G.; Chen, L. *Solid State Commun.* **2001**, *119*, 143.
(21) Shao, M.; Zhang, W.; Wu, Z.; Ni, Y. *J. Cryst. Growth* **2004**, *265*, 318.
(22) Zhang, H.; Ji, Y.; Ma, X.; Xu, J.; Yang, D. *Nanotechnology* **2003**, *14*, 974.
(23) Liao, X.-H.; Wang, H.; Zhu, J.-J.; Chen, H.-Y. *Mater. Res. Bull.* **2001**, *36*, 2339.
(24) Cao, X.; Li, L.; Xie, Y. *J. Colloid Interface Sci.* **2004**, *273*, 175.
(25) Ye, C.; Meng, G.; Jiang, Z.; Wang, Y.; Wang, G.; Zhang, L. *J. Am. Chem. Soc.* **2002**, *124*, 15180.
(26) Wang, H.; Zhu, J.-J.; Zhu, J.-M.; Chen, H.-Y. *J. Phys. Chem. B* **2002**, *106*, 3848.

10.1021/cm0478733 CCC: $30.25
Published on Web 03/04/2005

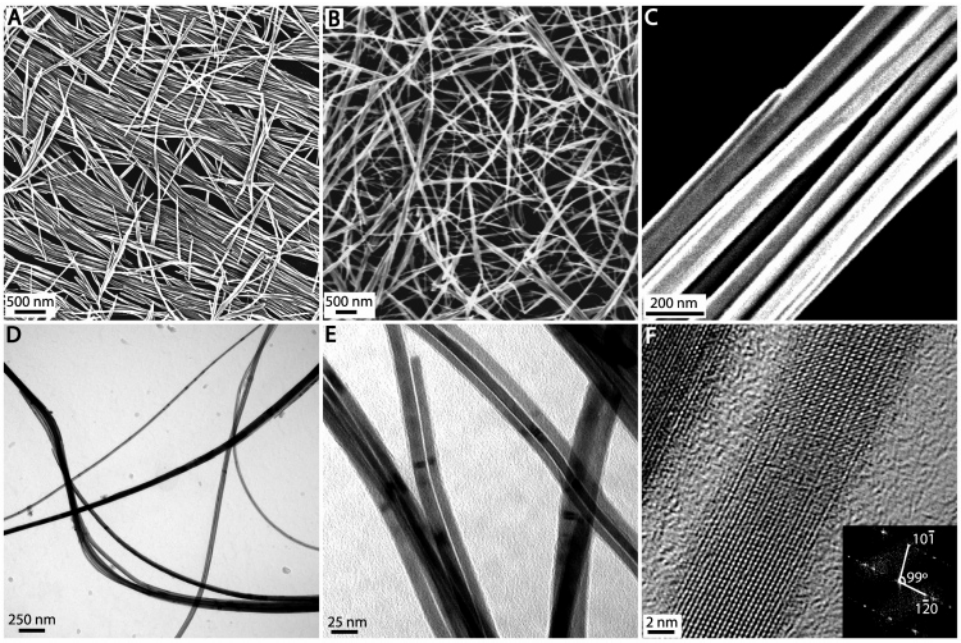

Figure 1. (A, B, C) SEM and (D, E) low-resolution TEM images of Bi_2S_3 nanowires. The wires range from 0.5 to 70 μm long, with the majority of wires longer than 5 μm. The average diameter was 26.0 nm ($\sigma = \pm$ 17.4 nm for 200 wires counted). (F) High-resolution TEM image of an 8-nm diameter nanowire; (Inset) FFT of the TEM image revealing that the nanowire growth direction is [002].

Materials and Methods

All chemicals were used as received from Aldrich Chemical Co. Water was doubly distilled and deionized.

Nanowire Synthesis. A 36-mL portion of 10.9 mM bismuth nitrate ($Bi(NO_3)_3$) [0.19 g] was mixed with 25 mL of chloroform ($CHCl_3$) with 0.42 g of sodium octanoate ($NaOOC(CH_2)_6CH_3$). In aqueous solutions, bismuth nitrate dissociates into ionic species ranging from $Bi(NO_3)^{2+}$ to $Bi(NO_3)_4^-$.[27] Negatively charged octanoate serves as a phase transfer catalyst for $Bi(NO_3)_{3-n}^{n+}$ ions, solvating them in the organic phase. Dodecanethiol ($C_{12}H_{25}SH$; 300 μL) was added, resulting in a bright yellow organic phase. The thiol forms a stronger complex with the Bi cations and the color change results from the charge-transfer complex formed as the thiol displaces the octanoate. Following 20−60 min of stirring, the organic phase was separated and then evaporated to leave a bright yellow waxy precursor material. The Bi_2S_3 precursor was heated for 1 h at 225 °C in air to produce a brownish/black solid composed of nanowires. At these temperatures, the sulfur−carbon bond cleaves to form a crystalline metal sulfide product. The product was dispersed in chloroform and centrifuged at 7000 rpm for 10 min to remove molecular byproducts from the reaction. The nanowire yield was ∼20% based on number of moles of Bi converted to Bi_2S_3.

Nanorod Synthesis. A 36-mL portion of 12.0 mM $Bi(NO_3)_3$ (0.21 g) was combined with a dispersion of 0.20 g of $NaOOC(CH_2)_6CH_3$ in 25 mL of $CHCl_3$. After 10 min of vigorous stirring, 0.18 g of elemental sulfur (S) was added. The mixture was stirred for 60 min with the organic phase becoming a faint yellow color. The organic phase was separated and dried on a rotary evaporator to leave a bright yellow waxy solid. Dodecanethiol (240 μL) was then added dropwise to the solid. One hour later, the waxy precursor material appeared as a dark red material: the thiol diffused into the solid and changed the color of the material. The precursor was heated for 1 h at 160 °C to produce a black solid containing nanorods. The product was redispersed in chloroform and precipitated by adding excess ethanol to remove unwanted molecular byproducts. The nanorod yield was ∼33% based on number of moles of Bi converted to Bi_2S_3.

Characterization. Transmission electron microscopy (TEM), scanning electron microscopy (SEM), X-ray diffraction (XRD), and selective area electron diffraction (SAED) were used to characterize the nanocrystals. Low- to intermediate-resolution TEM images were obtained digitally using a Philips 208 TEM operating at 80 kV accelerating voltage with an AMT Advantage HR model CCD camera. High-resolution TEM and SAED were performed using a JEOL 2010F TEM equipped with a field emission gun operating at 200 kV accelerating voltage. Images were acquired digitally on a Gatan multipole scanning CCD camera. Electron diffraction patterns were taken using a 10-μm diffraction aperture. All TEM samples were prepared by drop casting nanocrystals from chloroform onto 200-mesh carbon-film-coated Cu grids (Ladd Research) or 200-mesh lacey carbon-coated Cu grids (Electron Microscopy Sciences). SEM was performed on nanowire samples using a LEO 1530 field emission gun SEM operating at 1−3 kV accelerating voltage with digital image acquisition using an Inlens detector and LEO 32 software system. SEM images were obtained from nanorods and nanowires drop cast onto glassy carbon substrates (1 × 1 cm and 1 mm thick) from chloroform using a LEO 1530 field emission gun SEM at 1−3 kV accelerating voltage. Images were acquired digitally by an Inlens detector equipped with a LEO 32 software system. XRD was obtained from nanowires and nanorods drop cast from chloroform onto quartz (0001) substrates using a Bruker-Nonius D8 Advance θ-2θ powder diffractometer with Cu Kα radiation, Bruker Sol-X Si(Li) solid-state detector, and a rotating stage. XRD patterns were collected over an 8−12 h period with a 0.02° angle increment at a rate of 12°/min.

Results and Discussion

Control of Nanocrystal Aspect Ratio. Figure 1 shows TEM and SEM images of nanowires produced in this reaction. The nanowires are ∼25 nm in diameter with the majority exceeding 5 μm in length. The aspect ratio is greater than 100 and nanowires as long as 70 μm can be observed.

(27) Cotton, F. A.; Wilkinson, G. *Advanced Inorganic Chemistry*, 3rd ed.; John Wiley & Sons: New York, 1972.

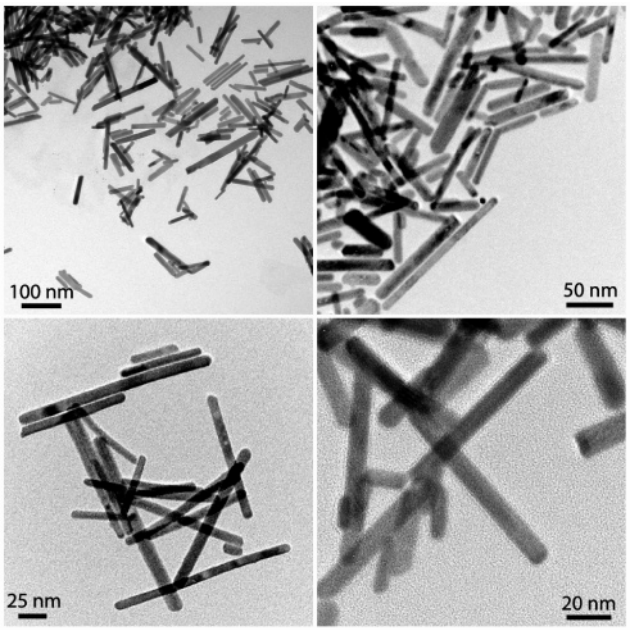

Figure 2. TEM images of Bi_2S_3 nanorods with an aspect ratio of ~7: average length and diameter of 73.6 nm ($\sigma = \pm$ 38.8 nm for 200 rods counted) and 10.7 nm ($\sigma = \pm$ 3.2 nm for 200 rods counted).

In the solventless reaction environment, the hydrocarbon chains from the octanoate and the decomposing thiolate confine nanocrystal growth to localized reaction volumes that do not mix to an appreciable extent, much like what occurs in confining media such as polymers, glasses, and zeolites. In the solventless media, however, the host material does not exhibit well-defined "pores" and rearranges around the precipitating material as it degrades during the reaction. The organic species adsorbs relatively strongly to the surface of the nanowires, providing dispersibility in organic solvents such as chloroform and hexane and nanometer-scale separation between neighboring wires. In fact, Bi_2S_3 nanowires appear to form as close-packed bundles, like those shown in Figure 1C−1E, with wires separated by an intervening organic layer.

The addition of elemental sulfur to the solventless reaction of the Bi alkylthiolate and octanoate mixture produces shorter aspect ratio nanorods. The highest quality product is obtained at significantly reduced reaction temperatures of ~160 °C, with nanorods that are on average ~10 nm in diameter and ~70 nm long, as shown in the TEM images in Figure 2. The nanorods readily disperse in organic solvents, such as chloroform and hexane, indicating that their surfaces are terminated with organic ligands.

Crystallographic Structure and Orientation. Both the nanowires and nanorods are composed of orthorhombic Bi_2S_3 (bismuthinite, JCPDS file 17-0320). The nanorod XRD patterns (Figure 3B) show no significant deviation in relative peak intensities from that of bulk bismuthinite. However, the diffraction patterns for the nanowires (Figure 3A) exhibit higher (101) peak intensity and decreased intensity of the merged (130)/(310) peaks. The relatively large differences in peak intensities indicate that the material is composed of aspherical crystalline domains that are elongated in a preferred crystallographic orientation.

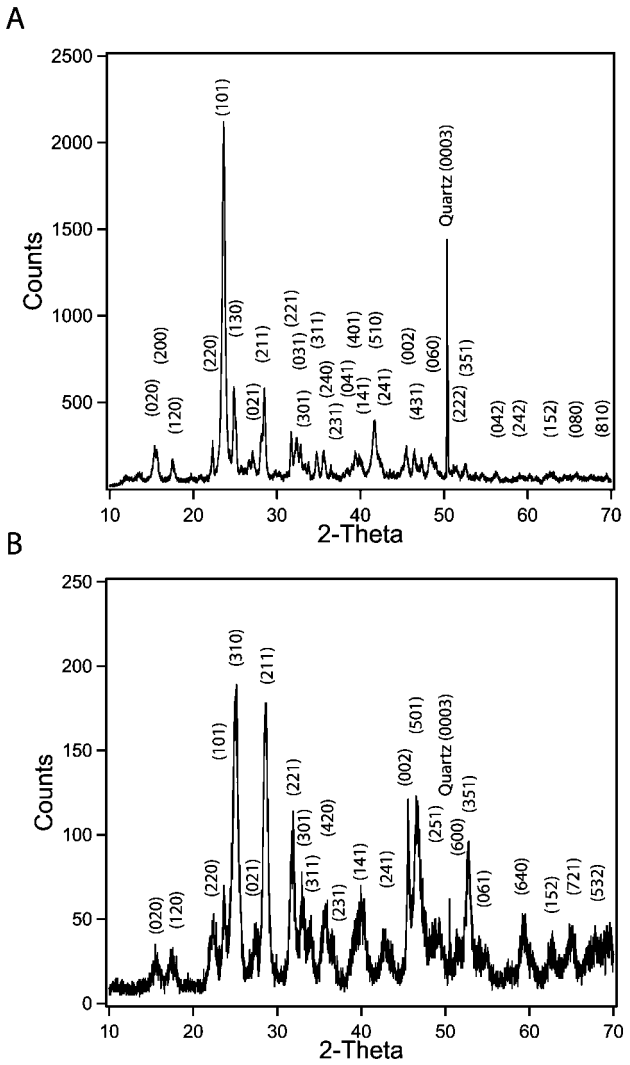

Figure 3. XRD obtained from Bi_2S_3 (A) nanowires and (B) nanorods. Both exhibit orthorhombic Bi_2S_3 crystal structure (bismuthinite, JCPDS file 17-0320).

Fast Fourier transforms (FFTs) of HRTEM images and selected area electron diffraction (SAED) patterns reveal that the nanowires extend preferentially in the [002] direction. For example, the FFT of the 8-nm diameter nanowire in Figure 1F is consistent with a nanowire elongated in the [002] direction with an electron beam incident along the [212] zone axis. To help interpret many of the FFT and SAED patterns, electron diffraction (ED) patterns were simulated with the JEMS software package using the appropriate lattice cell dimensions (11.149 × 11.304 × 3.981 Å) for orthorhombic Bi_2S_3 with the *Pbnm* (No. 62) space group with Bi and S atomic coordinates listed in Wyckoff.[28] Figure 4 shows examples of experimental SAED patterns compared to simulated diffraction patterns. Both nanowires in Figure 4 are elongated in the [002] direction. The nanowire in Figure 4A is oriented with its [120] zone axis perpendicular to the substrate, and as a result the {001} and $\{2\bar{1}0\}$ reflections appear in the SAED pattern parallel and perpendicular, respectively, to the [002] direction (the long axis of the nanowire), with the $(2\bar{1}\bar{1})$ reflection occurring at 52° from

(28) Wyckoff, R. W. G. *Crystal Structures: Inorganic Compounds*, 2nd ed.; Interscience Publishers: New York, 1964; Vol. 2.

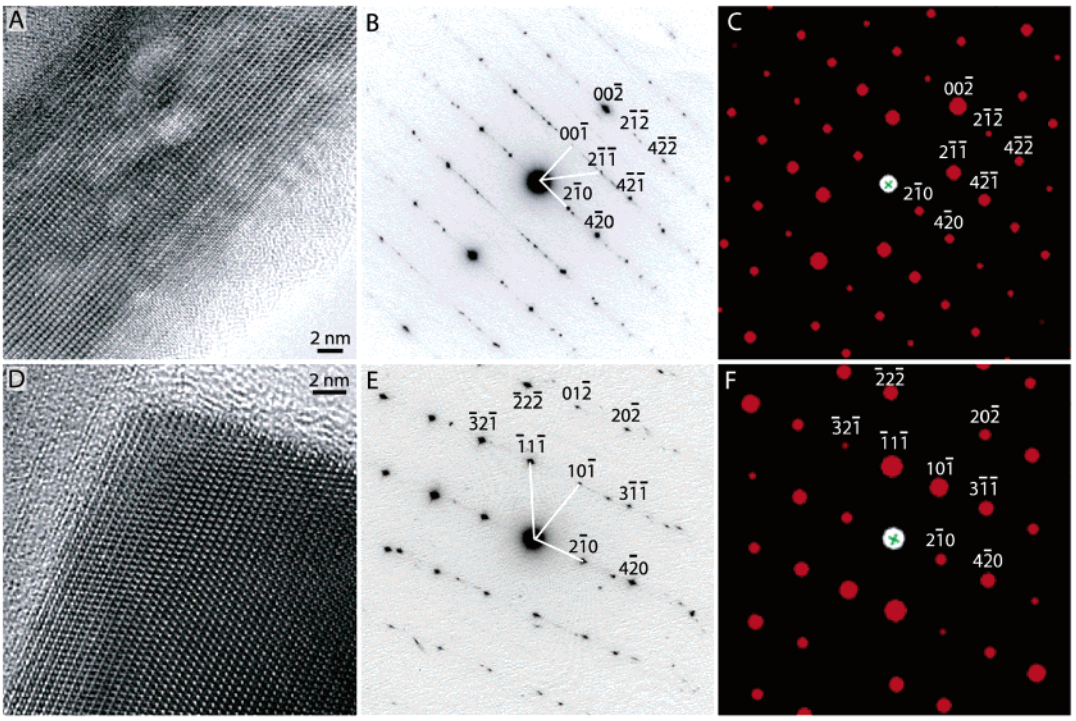

Figure 4. (A, D) HRTEM images of Bi_2S_3 nanowires with (B, E) SAED patterns obtained from the imaged area. The ED patterns match (C, F) electron diffraction patterns simulated with the electron beam oriented along the [120] and [121] zone axes, respectively, with the nanowires elongated in the [002] direction.

the $\{2\bar{1}0\}$ reflection. The nanowire in Figure 4D is oriented with its [121] zone axis perpendicular to the substrate. Therefore, the $\{2\bar{1}0\}$ reflections appear across the width of the wire and the $\{10\bar{1}\}$ and $\{\bar{1}1\bar{1}\}$ reflections appear at 73° and 115° from the $\{2\bar{1}0\}$ reflections. The {002} family of planes is oriented at 90° from the $[2\bar{1}0]$ direction (i.e., perpendicular to the growth direction) and 19.5° from the $[10\bar{1}]$ direction, consistent with a nanowire elongated in [002] direction. Note that no lattice reflections appear in the SAED pattern parallel to the long axis because of the particular crystallographic zone axis parallel to the incident electron beam. Of the 64 nanowires examined by SAED and/or FFT, all 64 were extended in the [002] direction.

It is worth noting a few unexpected features in the experimental diffraction patterns, as in Figure 4B, that result from the small size of the sample: (1) the kinematically forbidden (001) and $(00\bar{1})$ reflections appear, and (2) numerous faint reflections appear, representing noninteger fractions of the allowed reflections. These additional reflections are most likely due to breaks in crystal lattice symmetry such as monatomic steps and kinks along the nanocrystal surface.[29−31]

The Bi_2S_3 nanorods are also oriented with their long axes in the [002]. See for example, two representative nanorods in Figure 5 with their FFTs and the simulated ED patterns. The rod in Figure 5A is oriented on its [120] zone axis and as a result the {210} family of lattice reflections appears at 90° to the [002] growth direction. In Figure 5D, the electron beam is incident down the [110] zone axis of this nanorod

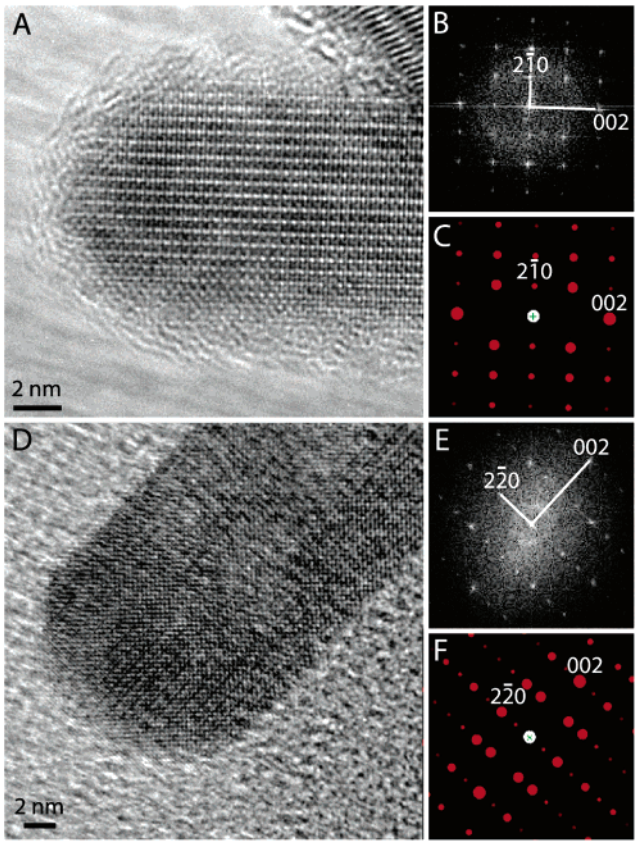

Figure 5. (A, D) HRTEM images and (B, E) corresponding FFTs of two Bi_2S_3 nanorods. (C, F) The ED patterns simulated for rods elongated in the [002] direction with the electron beam incident along the [120] and [110] zone axes, respectively, match the FFTs, and confirm the crystallographic orientation and growth direction of the nanorod.

and therefore the $\{\bar{1}10\}$ reflections occur across the short axis of the wire, perpendicular to the [002] direction. All of

(29) Gibson, J. M.; Lanzerotti, M. Y.; Elser, V. *Appl. Phys. Lett.* **1989**, *55*, 1394.
(30) Lynch, D. F. *Acta Crystallogr.* **1971**, *A27*, 399.
(31) Castaño, V.; Gómez, A.; Yacaman, M. J. *Surf. Sci.* **1984**, *146*, L587.

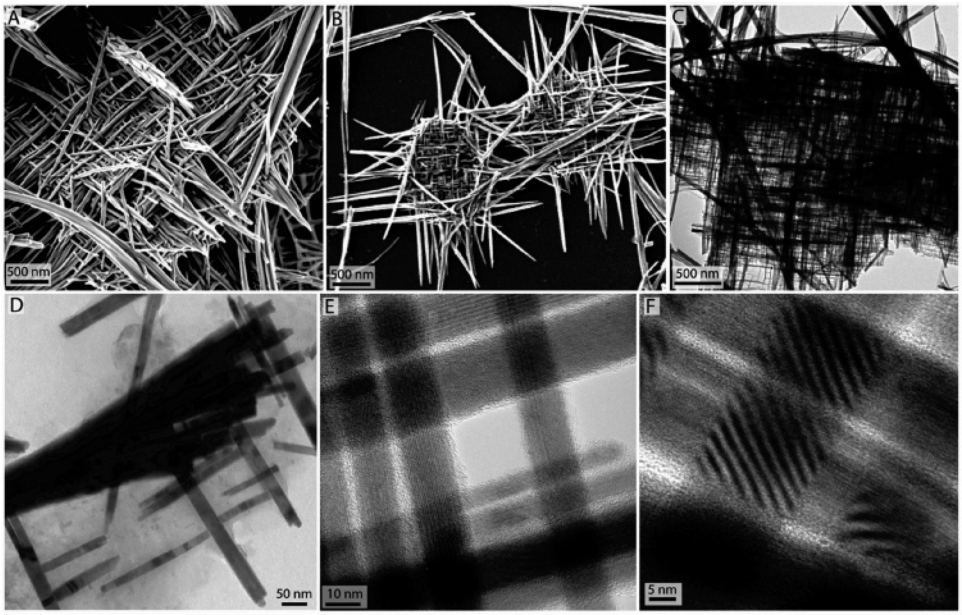

Figure 6. (A) and (B) SEM images of Bi_2S_3 nanofabric. (C) Low-resolution TEM image of nanofabric illustrating a high degree of order throughout the fabric over micrometer length scales. (D) Area of fabric in its initial stages of formation showing the nucleation of new wires at 90° relative to pre-existing ones. (E) Intermediate- and (F) high-resolution TEM images showing areas of densely ordered nanowires forming the inner mesh of the fabric.

the nanorods examined by HRTEM (26 of 26) were elongated in the [002] direction.

The addition of elemental sulfur to the reaction environment changes the nanocrystal growth kinetics significantly and "quenches" nanowire elongation. The sulfur−carbon bond in free dodecanethiol is relatively stable and will not break at 160 °C unless complexed with Bi. Therefore, the only way to increase the sulfur-to-bismuth ratio in the reaction is to add an independent sulfur source, i.e., elemental sulfur. The addition of free sulfur increases the rate of Bi_2S_3 formation, the thermodynamic driving force for nucleation,[32] and depletes the available Bi needed to extend the nanostructures to very long aspect ratios. Dodecanethiol plays an important role in nanorod formation, as poorly formed agglomerated particles resulted when it was not added to the reaction; however, it is the addition of free sulfur to the reaction that prevents nanowires from growing with very long aspect ratios, terminating growth to produce rods.

Formation of Nanofabric. Higher reaction temperatures (240 °C) also change the nanowire growth kinetics, resulting in different nanomaterial morphologies. At these higher synthetic temperatures, fabric-like structures form as an interlocking square lattice of interwoven nanowires exhibiting an extremely high degree of orientational order (Figure 6). The yield of these matted structures is relatively low (estimated at <1% of total nanocrystal mass); however, they occur reproducibly in all reactions. Furthermore, reactions at 225 °C rarely produced these kinds of structures. The fabrics typically consist of two interpenetrating layers of crossed nanowires as shown in Figure 6B and C that cover an area of $\sim 10\ \mu m^2$. Thicker fabrics with multiple layers of crossed nanowires could also be observed (Figure 6A). The nanowires in the fabric are densely packed with wire-to-wire separations as small as one nanometer (as in Figure 6E), and they exhibit a very high degree of perpendicular orientational order with very few misaligned nanowires. The nanowire fabrics form as a result of the epitaxial nucleation and growth of wires on wires that occurs at these temperatures.

In the fabrics, the nanowires exhibit crystallographic registry between crossed and parallel wires. As shown in Figure 6D, nanowires are found to grow from the surface of existing wires. Unlike hexagonally branched Bi_2S_3 snowflakelike structures observed by Lu et al. and Wang et al. in their hydrothermal syntheses, the Bi_2S_3 structures formed in the solventless environment exhibit perpendicular branching.[33,34] The "symmetry-breaking" results from the asymmetric Bi_2S_3 crystal structure and the epitaxial registry between crystallographic planes of crossed nanowires. FFTs of high-resolution TEM images (as in Figure 7A) of regions of crossed nanowires reveal two identical overlapping diffraction patterns oriented at exactly 90° with respect to one another. In order for this to occur, all of the wires in the image must be oriented with the same zone axis along the direction of the electron beam, in this case the [110] zone axis, with the same growth direction. The elongation of the nanowires in the [002] direction is revealed in the two {002} spots (1.99 Å spacing) in the FFT oriented perpendicular to each other. The $\{\bar{1}10\}$ lattice reflections from each nanowire in the FFT are oriented at an angle of 90° from one another as depicted schematically in Figure 7E. With the electron beam incident along the [110] zone axis, the $\{2\bar{2}\bar{1}\}$ and $\{\bar{2}2\bar{1}\}$ sets of lattice reflections appear at 45° from the $\{\bar{1}10\}$ and {002} lattice reflections, and therefore, with the nanowires perpendicularly oriented, the $\{2\bar{2}\bar{1}\}$ and $\{\bar{2}2\bar{1}\}$ diffraction spots overlap exactly in the FFT. The parallel

(32) Toschev, S. Homogeneous Nucleation. In *Crystal Growth: An Introduction*; Hartman, P., Ed.; American Elsevier: New York, 1973; Vol. 1.

(33) Lu, Q.; Gao, F.; Komameni, S. *J. Am. Chem. Soc.* **2004**, *126*, 54.

(34) Wang, D.; Shao, M.; Yu, D.; Yu, W.; Qian, Y. *J. Cryst. Growth* **2003**, *254*, 487.

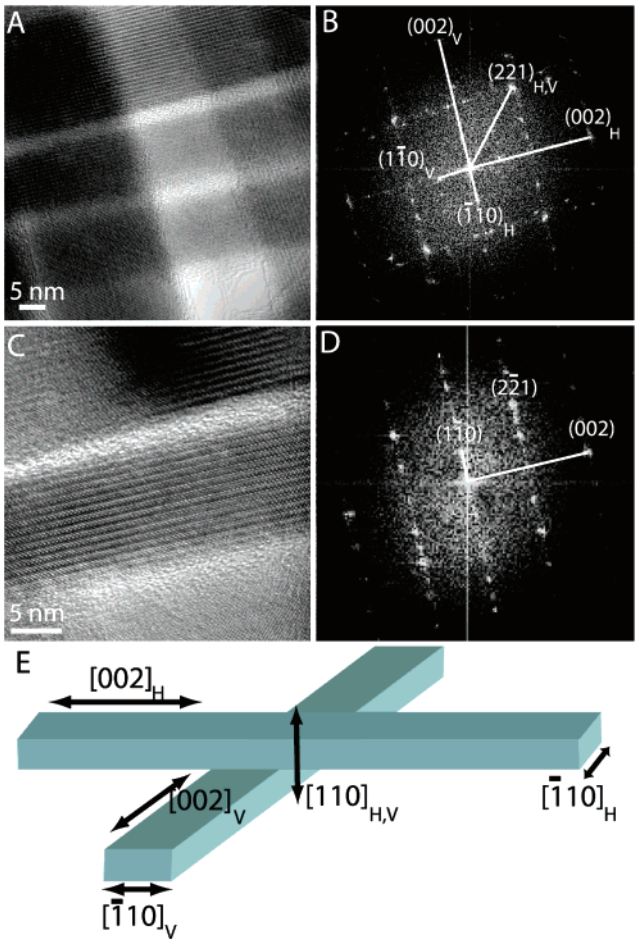

Figure 7. (A) HRTEM image and (B) corresponding FFT of the image reveals the precise crystallographic registry between crossed nanowires in the fabric. The FFT shows the overlapping patterns of the crossed nanowires—the FFTs match simulated electron diffraction from the [110] zone axis (for example, see Figure 3F). (C) Magnified HRTEM image of the three horizontally oriented nanowires imaged in (A); and (D) the FFT of the imaged region containing all three nanowires shows that all three wires are crystallographically oriented with respect to their [110] zone axes.

nanowires also exhibit crystallographic registry indicating that they originated from the surface of the same nanowire. Figure 7C shows a magnified image of the three parallel wires in Figure 7A. The FFT of the image shows spots as expected from a single perfect crystal with the beam incident along the [110] zone axis. The extent of crystallographic registry between crossed nanowires in the fabric results from the heterogeneous seeding of nanowires and their "epitaxial" growth.

The crossed nanowire growth appears to originate from a lattice defect, as Moiré fringes (Figure 6F) at the crossed nanowire junctions reveal that the two nanowires do not exhibit the same crystallographic orientation.[35,36] The nanowires in the fabric are all elongated in the [002] direction and are oriented with their [110] zone axes perpendicular to the substrate. At the nanowire junction, both of the crossed nanowires are oriented with their {110} lattice planes parallel to the substrate (perpendicular to the [110] direction). A rotation of the orthorhombic Bi_2S_3 crystal lattice by 90° around the [110] direction produces two interfacing crystal domains with a small amount of lattice mismatch. The {220} and {440} lattice spacings (3.967 and 1.985 Å) running parallel to the growth direction are very close to the {001} and {002} lattice spacings (3.981 and 1.990 Å) perpendicular to the growth direction. Furthermore, the $\{2\bar{2}\bar{1}\}$ and $\{\bar{2}2\bar{1}\}$ sets of lattice planes oriented at 45° from the $\{\bar{1}10\}$ and {002} lattice reflections have no lattice mismatch for orthogonally oriented wires. Therefore, despite the difference in crystallographic orientation the crossed nanowires exhibit minimal lattice distortion at their junction and heterogeneous growth of crossed nanowires is favored in this system at high synthetic temperatures.

Conclusion

The synthesis of high aspect ratio orthorhombic Bi_2S_3 (bismuthinite) nanowires by Bi alkylthiolate thermolysis shows that the solventless approach to nanomaterials precipitation has the potential for producing a wide range of morphologies, from spherical particles, disks, rods, prisms, and wires. The asymmetric nanocrystal shape reflects the asymmetric crystal structure of the solid, and differences in crystal growth kinetics as a function of crystallographic orientation have been found to be important in the solventless environment. The addition of "free" chemical species, such as elemental sulfur, into the reaction mixture can be used to change the growth kinetics and provides a potential route for obtaining general shape tunability in the solventless environment.

Acknowledgment. We thank José Luís Elechiguerra for assistance with the electron diffraction simulations. We acknowledge the National Science Foundation, the Welch Foundation, and the Texas Higher Education Coordinating Board through its ATP program for partial financial support of this work.

CM0478733

(35) Williams, D. B.; Carter, C. B. *Transmission Electron Microscopy: A Textbook for Materials Science*; Plenum Press: New York, 1996.

(36) Based on the measured spacing, d_M of 24.3 Å between Moiré fringes in Figure 6F, the mismatch between the {002} lattice planes along the length of one wire and the {440} lattice planes across the width of the second indicates a rotational shift between the two crystal lattices of the wires of 2.3° (i.e., wires are 87.7° apart) as determined by the following equation $d_M = (d_1 d_2)/((d_1 - d_2)^2 + d_1 d_2 \beta^2)^{1/2}$ for Moiré fringes with both translational and rotational mismatch, with d_1 and d_2 being the spacing between the two sets of planes, and β being the degree of rotation between the two sets of planes. This calculated rotation between crystal lattices is comparable to the measured value of 87° between the actual wires in Figure 6F. Bulk values of 1.99 Å for the {002} planes and 1.985 Å for the {440} planes were used in the calculation to represent the translational mismatch between lattice fringes of the two crossing wires.